This paper was published in Geothermics, 51, 270-280, (2014),
doi:10.1016/j.geothermics.2014.01.016.

Economic evaluation of geothermal reservoir performance through modeling the complexity of the operating EGS in Soultz-sous-Forêts

Sebastian Held*[1], Albert Genter[2], Thomas Kohl[1], Thomas Kölbel[3], Judith Sausse[4], and Martin Schoenball[5]

[1] *Karlsruhe Institute of Technology, Institute of Applied Geosciences, Karlsruhe, Germany*
[2] *GEIE Exploitation Minière de la Chaleur, Kutzenhausen, France*
[3] *EnBW Energie Baden-Württemberg AG, Karlsruhe, Germany*
[4] *Département Geosciences, Nancy Université, Bld. des Aiguillettes, Vandoeuvre les Nancy, France*

Abstract

The EGS pilot project in Soultz-sous-Forêts, is now operated by an industry consortium, heading for optimal reservoir management.

A 3D thermo-hydraulic numerical model, based on a complex geological model of the reservoir is presented with the goal to determine input parameter for an economic analysis, comparing reservoir management based on levelized cost of energy.

Over the projected life time of 30 years no major thermal breakthrough is predicted, small temperature decline affects net energy output only negligibly. The results highlight the benefits of multi-well systems, offering a larger heat exchanger surface and higher flexibility for reservoir management.

1 Introduction

Geothermal energy has strong assets over other renewables due to its huge worldwide potential and its base-load capacity. However, especially in low temperature areas, geothermal still has to prove its competitive capacity against other renewables in terms of economic profitability. Recent data for geothermal power production shows that the levelized cost of energy in the German low enthalpy region using binary cycle technology varies from 0.17 to 0.27 Euro/kWh [Kölbel

*sebastian.held@kit.edu

et al., 2011]. A major perspective is attributed to Enhanced Geothermal Systems (EGS) since they have the potential to be applied in the deep crystalline basement containing the largest geothermal resource [Tester et al., 2006; IEA, 2011]. Parallel to the technical developments of these systems, economic analyses have to be performed to highlight its current state of development. Since there is little world-wide experience in the field of EGS, site-specific analyses have to be performed. The current EGS project and former European geothermal pilot plant Soultz-sous-Forêts provides a large data base from its long research history but requires state-of-the-art planning strategies for future operation. Exploration of this EGS project began in 1986 and was mainly based on field data (geology, temperature, seismic profiles) from the old Pechelbronn oil field. The project was aimed at designing a deep seated heat exchanger, which allows producing power from low permeable basement rocks. With an industrial consortium (GEIE) entering the project in 2001 [Genter et al., 2010] an economic viability was requested, beside the ongoing research. An ORC (Organic Rankine Cycle) pilot power plant was built in 2008 to start the production of electricity. Geothermal 200 °C. energy has strong assets over other renewables due to its huge world-wide potential and its base-load capacity. However, especially in low temperature areas, geothermal still has to prove its competitive capacity against other renewables in terms of economic profitability. Recent data for geothermal power production shows that the levelized cost of energy in the German low enthalpy region using binary cycle technology varies from 0.17 to 0.27 Euro/kWh [Kölbel et al., 2011]. A major perspective is attributed to Enhanced Geothermal Systems (EGS) since they have the potential to be applied in the deep crystalline basement containing the largest geothermal resource [Tester et al., 2006; IEA, 2011]. Parallel to the technical developments of these systems, economic analyses have to be performed to highlight its current state of development. Since there is little world-wide experience in the field of EGS, site-specific analyses have to be performed. The current EGS project and former European geothermal pilot plant Soultz-sous-Forêts provides a large data base from its long research history but requires state-of-the-art planning strategies for future operation. Exploration of this EGS project began in 1986 and was mainly based on field data (geology, temperature, seismic profiles) from the old Pechelbronn oil field. The project was aimed at designing a deep seated heat exchanger, which allows producing power from low permeable basement rocks. With an industrial consortium (GEIE) entering the project in 2001 [Genter et al., 2010] an economic viability was requested, beside the ongoing research. An ORC (Organic Rankine Cycle) pilot power plant was built in 2008 to start the production of electricity.

When the Soultz-sous-Forêts project started around 1990 as a research facility, economical concerns were not the main interest of the project. But today, after a rapid development of the sector and beginning investor interests the consideration of economic aspects is essential. Main advantages of economic analyses are sensitivity investigation to support management decision.

The Soultz site is located next to the western boundary fault of the Upper Rhine Graben (URG), formed in the context of the European Cenozoic rift

system in association with the alpine orogenesis [Ziegler, 1994]. The site is located on the Soultz horst structure, where the granitic basement rocks are covered by only 1400 m of Mesozoic and Cenozoic sediments. In comparison with other geothermal sites, the Soultz reservoir is exceptionally well explored. Dezayes et al. [2004] and [2010] identify the dominating fractures controlling the fluid flow in the reservoir. Based on this work and further investigations, Sausse et al. [2010] set up a 3D local geological model of the reservoir, whereas Baillieux et al. [2011] develop a 3D regional geological model, describing mainly the large-scale faults appearing in this part of the URG.

In addition to the structural assessment, an economic consideration of the Soultz reservoir requires quantitative estimates of temperature and flow rate development. Therefore, a reservoir model has to be established that characterizes especially flow behavior and structural properties in subsurface, linking current measurements to quantitative forecasting of future conditions. Out of a large number of models developed, the following selection summarizes these numerical modeling efforts at Soultz of the last years. Applying the FRACAS code with a discrete fracture network (DFN) approach, Baujard and Bruel [2006] focus on the coupling of mechanical and hydraulic processes including density effects between reservoir and injected fluid in the deeper reservoir. Calibration was done using hydraulic data and the location of microseismic events caused by hydraulic stimulation. Besides providing improved hydro-mechanical characterization of the fractured reservoir, the hydro-mechanical interactions during stimulation could be simulated by their model. Investigating flow and transport in the deeper reservoir Blumenthal et al. [2007] applied a simplified 2D model using the SHEMAT code. They described the most dominant deterministic fractures and two fracture family sets. Calibration was performed from tracer tests experiment between GPK3 and GPK2/GPK4, which were carried out in 2005 [Sanjuan et al., 2006]. Breakthrough time and maximum tracer concentration was reproduced quite well, but tailing and final tracer concentration data could not be matched well. This model was also applied to predict the long-term temperature changes under operation conditions, resulting in a temperature drawdown after one year and a near steady state after 20 years with up to 80 °C cooler production fluids. Kohl and Mégel [2007] created a DFN-type numerical model of the deeper Soultz reservoir to investigate the hydro-mechanical behavior under stimulation conditions. The model was applied to a GPK4 hydraulic experiment from 2004. The hydraulic-mechanical HEX-S model designed on basis of the experience of the stimulation and testing data from the other wells allowed predicting the reservoir pressure response and the shearing locations during the first day of stimulation. More recent modeling efforts from Gentier et al. [2010] are based on a discrete 3D fracture network, which consists of four main fracture sets according to the fracture orientations found in Soultz. The hydraulic properties of the fracture network were calibrated using hydraulic and tracer data, based on the model of the deeper reservoir by Baujard and Bruel [2006]. Both measured tracer breakthrough curves in GPK2 and GPK4 could not be fitted with a single model. Furthermore, the model did not take into account the occurrence of casing leakages in GPK2 and in GPK4, which are

suspected to contribute strongly to the flow pattern [Jung et al., 2010]. Further attempts to fit the tracer test from 2005 have been conducted by Kosack et al. [2010] by deterministic Bayesian inversion using simplified 3D geometries with the SHEMAT simulator. The final model consists of zones of different permeability along the direct connection between GPK2 and GPK3, thus distinguishing areas of different degrees of stimulation and the virgin rock matrix. The modeled breakthrough curve for GPK3 fits quite well, but some alternative models produce almost equal results for the breakthrough curve, so that uniqueness of the results cannot be guaranteed.

Also using SHEMAT, Vogt et al. [2012a, 2012b] use both, a massive Monte Carlo (MC) attempt and the Ensemble Kalman Filter (EnKF) technique, in order to rebuild the permeability distribution in the deeper Soultz reservoir assuming a heterogeneous equivalent porous medium. Reliable fits of tracer test curves from 2005 for both wells GPK2 and GPK4 were only obtained by the EnKF technique. Based on their obtained permeability distribution no major thermal breakthrough is predicted within 50 years. Sulzbacher and Jung [2005] elaborated a simplified symmetric 3D model to simulate the temperature changes in the reservoir during operation. The cooling in the deeper reservoir was calculated using the ROCKFLOW code assuming a fault system consisting of four major structures. Being calibrated from hydraulic pressure data, the model anticipates a rapid decline in production temperature after a few years from the cooling of the reservoir due to re-injection.

Sanyal and Butler [2005] connect numerical calculations with a profitability analysis. Focus is on the development of guidelines to optimize EGS reservoir management. A finite difference approach, that includes matrix and fracture fluid flow, is used. They compare the impact of varying well numbers and stimulation campaigns with the help of produced net energy generation over a lifetime of 30 years. Highlighted are the effects of stimulated volume, production rate and number of wells on the net power generation. Kruck et al. [2011] use the annuity method [VDI, 2010] to calculate economic profitability of a geothermal project.

In this paper we develop a workflow from a complex 3D geological model to estimate and optimize the levelized cost of energy. Starting from an existing geological model of the Soultz reservoir [Sausse et al., 2010], a numerical thermo-hydraulic coupled model was created, focusing on observed hydraulically active faults and fractures. Results of long-term circulation simulations are fed into an economic model based on the annuity method. Using a catalog of 15 different reservoir management scenarios (only the most different scenarios are shown in this publication), we find the most profitable scenario for power generation. This comparison should improve future reservoir management with the target of economic efficiency and sustainability.

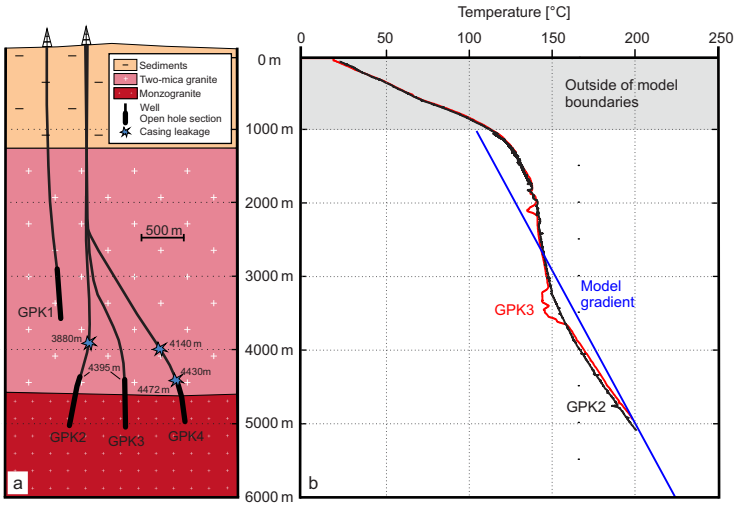

Figure 1: (a) Simplified deep geology, well trajectories and location of open-hole sections and leakages in the Soultz reservoir, (b) temperature profile in GPK2 and GPK3 and the initial temperature profiles assumed in the numerical model.

2 The Soultz EGS reservoir

The reservoir in Soultz is penetrated by four operating wells (Figure 1) and additional monitoring wells. First, believing in a constant geothermal gradient, GPK1 and the exploration well EPS1 were drilled up to 2 km depth. To reach higher temperatures GPK1 was deepened to 3600 m and GPK2 was drilled up to 3880 m depth [Genter et al., 2010]. These wells penetrate the so-called upper reservoir [Cuenot et al., 2006]. Through a deepening of GPK2 and drilling of GPK3 and GPK4 to over 5000 m depth, the deeper reservoir could be developed. Both reservoirs were stimulated to enhance the rock permeability [Gérard et al., 1997, Dorbath et al., 2009]. Recent operation plans consider all four GPK wells for fluid circulation. The lowest 500-700 m of the wells are open-hole sections without any casing. Casing restriction and leakages were detected in GPK2 and GPK4 [Cantini 2006, Pfender et al., 2006] (Figure 1). Their origin, which is still debated, could be a combination of post-stimulation shearing and local corrosion. The leakages allow reservoir fluids to enter the wells apart from open-hole sections. The casing restriction in GPK2 at 3880 m is associated to a large cave created by drilling operations. This cave is spatially associated with a large fractured and altered zone outlined from geological observations [Genter et al., 1999]. This casing restriction connects the upper reservoir to fluid production. Jung et al. [2010] estimated that about 15% of the whole production of GPK2 is due to this feature located at 3880 m. Leakage occurrence in GPK4 was investigated by Cantini [2006] with the help of different logging techniques such as acoustic image logs used for casing inspection. He could find evidences for

leakages in the well. The leakage location was confirmed by borehole image logs, which were run before installation of the casing in GPK4.

The three deep wells have a separation of around 650 m at 5 km depth aligned NNW-SSE, GPK1 and GPK2 are separated by 450 m of granitic rocks. Since the site is located on the Soultz horst, the granitic basement is reached in only 1400 m depth. The wells are drilled into the western faulted flanks of the horst, there the basement rock is supposed to contain more permeable fractures. Magnetotelluric measurements of Geiermann and Schill [2010] show a significant conductive anomaly at a depth down to 2000 m in the area of the Soultz and Kutzenhausen faults. It is interpreted as an abundance of highly permeable natural fractures.

The sediments above the granites are related to the geological evolution of the URG from late Paleozoic. The granitic basement is roughly divided in an upper porphyritic monzogranite down to 4800 m depth, followed by fine grained two-mica granite [Hooijkaas et al., 2006]. The granite massif is characterized as a low permeable but naturally fractured rock, in which a small-scale fracture network is linked to major faults or fractures [Dezayes et al., 2010]. In this paper, the term "fracture" is used for structures detected by logging measurements whereas a "fault" is used for large-scale structures with a suspected lateral displacement. The natural permeability is mostly linked to fracture systems. Through hydraulic or chemical stimulation, its permeability can be increased. E.g. an up to twentyfold increase of the productivity of GPK2 could be achieved [Schindler et al., 2008]. The existing fault systems must be seen in the context of the geological and tectonic history of the URG. The dominant fracture orientation ($160° \pm 15°$) at the Soultz site follows the present-day main horizontal stress of about $170° \pm 14°$ [Cornet et al., 2007]. Two other fracture sets, striking $20° \pm 10°$ (Rhenish) and $130° \pm 10°$ (Hercynian) compliment the dominant structure orientations [Dezayes et al., 2010]. A high inclination of over 60° mostly to the west is typical for the two fractured reservoirs.

The project is located on a thermal anomaly with a temperature gradient in the sedimentary cap of > 0.1 K/m (Figure 1b) [Haas and Hoffmann, 1929]. Below 1 km depth the gradient decreases strongly to 0.007 K/m. Le Carlier et al. [1994] assume this lower gradient being result of a convective cell between 1000 m and 3500 m depth. Permeability values of $> 1 \times 10^{-14}\,\mathrm{m}^2$ in the fractures in the granitic rock were estimated for such a convection cell [Bächler et al., 2003]. Beneath 3500 m depth, the typical geothermal gradient of about 0.03 K/m is observed. The hydraulic characteristics of the deeper reservoir were explored with the help of tracer tests [Sanjuan et al., 2006]. The tracer was injected in GPK3 while GPK2 and GPK4 were produced. The tracer breakthrough curve measured in GPK2 shows a very fast first arrival of the tracer and a long tailing with high concentrations of the tracer, indicating a direct connection between GPK2 and GPK3, which could be caused by a large fracture zone connecting the open-hole section from GPK3 with the casing restriction in GPK2. The long tailing indicates, that parts of the produced fluids migrate along a larger loop through the fracture system [Sanjuan et al., 2006]. In contrast the absolute tracer concentration in GPK4 is very low compared to GPK2, with a late first

arrival and a slowly increasing concentration. This indicates that the direct connection between GPK3 and GPK4 is impeded and the fluids between these wells have to migrate through the matrix. The relatively low rate of total recovery indicates that a lot of tracer vanishes into the open reservoir and leaves the circulation loop.

3 Geological Model

The geological 3D model by Sausse et al. [2010] and Place et al. [2011] is used as a basis for our numerical modeling. It bases on numerous data interpretation, such as petrography, hydrothermal alteration and natural fracture network characterization compiled from a geological database [Genter et al., 1995], well logs [Dezayes et al., 1995, 2005, 2010, Sausse and Genter, 2005, Sausse et al., 2006], microseismicity recordings [Cuenot et al., 2007, 2008, Dorbath et al., 2009] and Vertical Seismic Profiling (VSP) [Place et al., 2010, Place et al., 2011]. The main geophysical well logging run in the three deepest wells (GPK2, GPK3 and GPK4) consisted of the spectral gamma-ray log. Fracture geometrical properties and their spatial relationships were analyzed based on amplitude and transit time anomalies derived from acoustic image logs. Fractures can be identified with high accuracy and measured in azimuth and dip by this borehole imagery technique. Since 2003, other flow and/or temperature logs were run in the different deep wells during injection and production tests and some interpretation of the main fracture and permeable zones is proposed by Dezayes et al. [2005 and 2010]. These hydraulically active fractures correspond to either isolated fractures or series of thin parallel fractures or large-scale fracture zones. Further VSP data of the 1993 survey has been re-interpreted in GPK1 and EPS1 after a specific processing [Place et al., 2010]. Thanks to a high signal/noise ratio of these records, polarization analysis has been carried out: the arrivals show much more energy on the vertical component than on the horizontal components, suggesting a vertical polarization. At the well location, these seismic events are recognized at depth levels where the GPK1 well intersects highly permeable faults [Evans et al., 2005]. Finally, numerous hydraulic stimulations have been performed at Soultz between 2000 and 2005 and have generated microseismic activity that has been interpreted in terms of major structures. Events locations from Dorbath et al. [2009] were put into relation with the fault organization.

The model defines 53 structures in the vicinity of the geothermal plant and between depths of 800 to 6000 m below sea level. These are 39 fracture zones, 8 microseismic structures and 6 VSP-derived structures (Figure 2). For the thermal-hydraulic coupled reservoir model a sub-selection was made to determine the most dominating hydraulically active faults to reduce the complexity of the model to a manageable amount. Focusing on fractures with a dominant impact on flow in the reservoir, flow and temperature logs were evaluated to identify one or two fractures in each open-hole section with the greatest impact on the flow. Therefore all flow and temperature logs of GPK1-GPK4 were

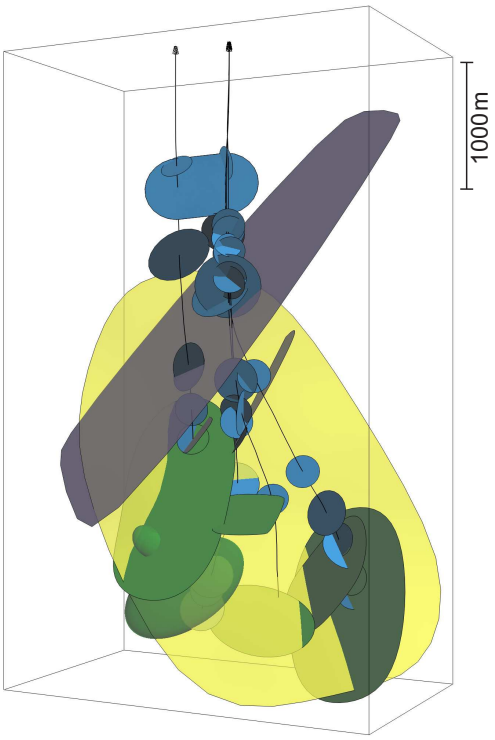

Figure 2: Geologic model of the Soultz reservoir [Sausse et al., 2010]. Blue: fractures from well logs; Green: fractures from microseismicity recordings; Lila: fractures from Vertical Seismic Profiling (VSP); Yellow: GPK-FZ4770*.

screened manually and zones with major hydraulic impact were identified. Only fractures with a major impact on the flow log were accounted for. In the GPK3 flow log in Figure 3 two major fractures can be identified at depths of 4770 m and 5020 m. They correspond to fractures GPK-FZ4770* and GPK3-FZ5020 as defined in Sausse et al. [2010]. These fractures were incorporated in our numerical model. Fractures with lower impact on fluid flow, e.g. the fracture which can be identified as MS-GPK3-2003c [Sausse et al., 2010], were not considered in our numerical model.

In Figure 3 steps at the temperature profile indicate zones, where different fluids entering the well. Furthermore flow logs were used to estimate the contribution of each fracture to the total amount of fluid entering the well. Flow or temperature anomalies in the casing parts were checked with the help of borehole image logs, being run before the casing installation. Orientations of permeable fractures were analyzed with respect to the regional stress field [Cornet et al., 2007] to define, whether the fracture is open, closed or critically stressed [e.g. Barton et al., 1995]. Therefore structures orientated sub-parallel to maximum horizontal stress were preferentially chosen. In order to reduce

Structure	Dip direction	Dip	Linked to open-hole section	Limited by	Transmissivity [m^2]
Kutzenhausen fault	N291°	49°	-	-	6.80×10^{-4}
Soultz fault	N263°	63°	-	Kutzenhausen fault	6.80×10^{-5}
Hermerswiller fault	N90°	78°	-	-	6.80×10^{-6}
GPK3-FZ4770*	N234°	71°		Kutzenhausen, Soultz and Hermerswiller faults	4.80×10^{-5}
GPK3-FZ4770* in the vicinity of GPK2	N234°	71°	GPK2		6.10×10^{-5}
GPK3-FZ4770* in the vicinity of GPK2	N234°	71°	GPK3		2.94×10^{-5}
MS-GPK4-20045b	N257°	85°	GPK4	Soultz fault	4.00×10^{-5}
MS-GPK2-2000a	N244°	86°	GPK2	MS-GPK4-20045b, Kutzenhausen fault, GPK4-FZ4770*	6.10×10^{-5}
MS-GPK3-2003a	N257°	63°	GPK1	GPK1-FZ2120, PS3-int (VSP), GPK4-FZ4770*	3.90×10^{-4}
GPK3-FZ5020	N22°	66.5°	GPK3	GPK4-FZ4770*, MS-GPK2-2000a, MS-GPK4-20045b	1.68×10^{-5}
GPK4-FZ4710	N212°	50°	GPK4	MS-GPK4-20045b, GPK4-FZ4770*, PS3-int (VSP), Soultz fault	4.00×10^{-5}
PS3-int (VSP)	N329°	63°	-	Kutzenhausen fault , GPK1-FZ2120, GPK-FZ4770*	2.80×10^{-5}
GPK1-FZ2120	N65°	70°	-	Kutzenhausen fault, GPK-FZ4770*, MS-GPK4-20045b	3.80×10^{-4}

Table 1: Subset of the 3D geological model [Sausse et al., 2010] selected for the numerical reservoir model, hydraulic properties and the connection to the wells and the fault network.

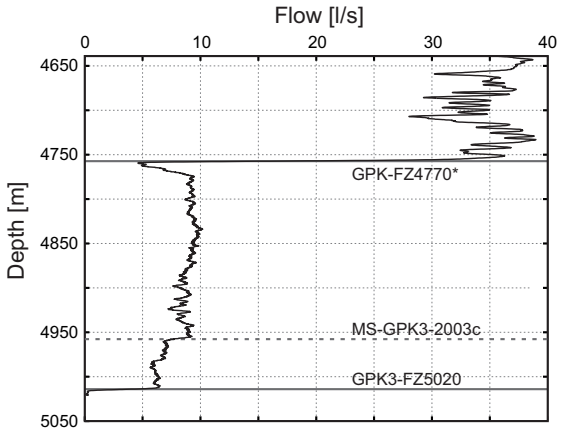

Figure 3: Flow log of the open hole section of GPK3.

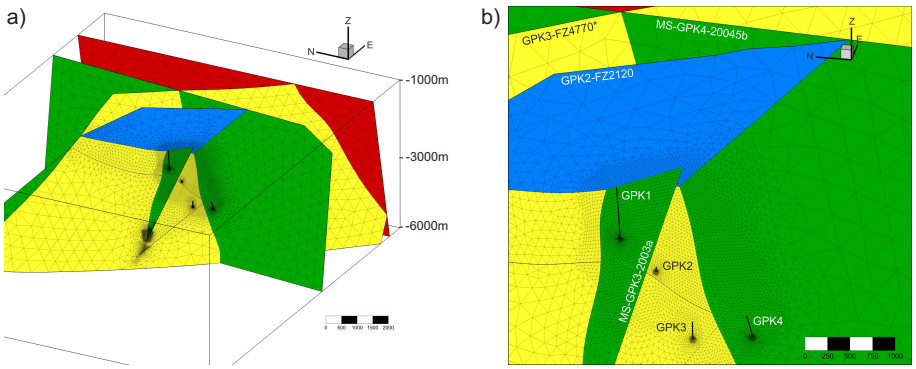

Figure 4: (a) Created finite element mesh of the simplified model. (b) Detail view of the generated mesh highlighting the different mesh sizes. Following fractures are not shown: Kutzenhausen fault, Soultz fault, PS3-int, GPK4-FZ4710.

the complexity of the geological model, the number of considered fractures was decreased to eleven, which are presented in Table 1 and Figure 4. The selected fractures were extended to the model boundaries or until they are cutoff by another fracture, in order to create a connected fracture network. The complex large-scale faults defining the local horst, taken from the model by Baillieux et al. [2011], were for the purpose of simplification, replaced by 2D planar surfaces. Almost all fractures inside the reservoir were cut by the most dominating fracture GPK-FZ4770* connecting GPK2 and GPK3. Each open-hole section is connected to the fracture network by two fractures except for GPK1, which is only connected by MS-GPK3-2003a.

In the Soultz reservoir the fluid flow in the matrix is dominated by small scale fractures. Sardini et al. [1997] determine the permeability of the fresh granite to

$4 \times 10^{-19}\,\mathrm{m}^2$, Sausse et al. [2006] calculated the permeability out of geophysical logs and give a value between $8.6 \times 10^{-18}\,\mathrm{m}^2$ - $9.6 \times 10^{-16}\,\mathrm{m}^2$ for the permeability depending on the degree of alteration. Hettkamp et al. [1999] have shown that matrix permeability and fracture permeability range from 10×10^{-18} to $1 \times 10^{-20}\,\mathrm{m}^2$, and 1×10^{-15} to 1×10^{-17}, respectively. Permeability values derived from pressure oscillation tests in the Soultz wells having a 700 m open-hole section, range between 1×10^{-14} and $4 \times 10^{-19}\,\mathrm{m}^2$ [Hettkamp et al., 1999]. Hence the observed permeability is about two orders of magnitude larger, than that of the fresh granite. Some numerical approaches consider small scale fractures [e.g. Gentier et al., 2010]. In our approach these fractures are not explicitly implemented to reduce complexity. Instead, a global matrix permeability is implemented in the model, representing the flow through the small scale fractures. We use an anisotropic permeability tensor with higher permeability in N-S direction to account for the preferential orientation of fractures in the regional stress field. We do not consider the permeability increase or variability in the vicinity of fractures or wells, caused by alteration or hydraulic and chemical stimulation.

4 Numerical Modeling

After compiling a simplified geological model, we set up a coupled thermo-hydraulic numerical model to compute pressure changes and transient temperature changes, which are the input parameters for the economic model, computing the levelized cost of energy. For the numerical calculations the finite element program FRACTure [Kohl and Hopkirk, 1995] was used. The code is able to simulate hydraulic, thermal, transport and elastic processes with the possibility to implement 1D, 2D and 3D elements in the same numerical model. The finite element mesh was generated using the software Hypermesh (Altair Engineering, Inc.). The selected fractures were implemented as 2D triangular elements in a matrix composed of 3D tetrahedrons. Both element types have pressure and temperature as degrees of freedom. Optimal mesh sizes were obtained by a sensitivity analysis of the element size to ensure a sufficient accuracy to simulate the steep pressure gradient around wells. Elements in the direct vicinity of the wells have a size of less than 3 m. Further away from the wells the typical element size reaches 40 m, increasing to 500 m in the far-field (Figure 4). 2D fracture elements are hydraulically characterized by a transmissivity, whereas for 3D matrix elements permeability is defined. Matrix elements which are in contact with fracture elements, share nodes with the two adjacent tetrahedrons.

Open parts of the well, i.e. open-hole sections and the leakages in the casings of GPK2 and GPK4, are represented by 1D line elements. In GPK2 the large distance between the leakage and the open-hole section was connected by a single line element, to prevent fluid flow between casing and rock matrix. The temperature increase of the injection fluid along the casing along this single line element is neglected. Details of the finite element mesh are shown in Figure 4. The size of the model domain was chosen such, that the imposed boundary

conditions did not influence the modeling results. A model extension of 13 km (E-W), 11 km (N-S) and 5 km (vertical) was chosen, which ensures at least 4 km lateral distance from each well to the model boundary. In vertical direction the model starts at 1 km depth, reaching to 6 km depth, which is 1 km below the deepest sections of the wells. No major interactions between well and rock matrix above that 1 km depth are known. However, heat transmission further reduces the produced water's temperature. Therefore we subtract from the modeled production temperature a constant value of 20 K in the economic calculations to reflect the cooling process of the produced fluid by the rocks in the uppermost 1000 m. The heating of the re-injected water is not taken into account. This effect has no major importance to the produced fluid, as no thermal breakthrough is observed. The temperature and extent of the cooled volume is of minor importance for the final economic calculations. Fracture roughness leading to a tortuous fluid flow [Auradou, 2009], is neglected. Taking it into account would enhance the cool down of the produced water due to channeling accompanied by heterogeneous cooling of the matrix.

Hydrostatic conditions were assumed in the reservoir, setting the hydraulic head at the lateral model boundaries to zero (Dirichlet-type). Pressure changes were calculated in terms of excess pressure. A stationary pressure field was computed in order to save computation time. This is a reasonable simplification, as our simulations focus on the long-term circulation. The convective influenced temperature field at the Soultz site was integrated in the model by an artificial linear temperature gradient of 0.024 K/m through constant temperature boundary conditions on top and bottom surface of the model (Dirichlet-type). Thereby, the unperturbed temperature in the reservoir was closely matched, with a maximal temperature difference of 18 K near the top of the model at 1600 m depth (Figure 1b). This leads to a slight underestimation of temperature in the sedimentary cover and an overestimation in the deeper parts of the reservoir. However, the heat distribution in the central part of the reservoir was not affected. To capture the influence of different production scenarios, transient temperature fields with a steady-state pressure field were computed. Production and injection rates are implemented with Neumann-type boundary conditions at the uppermost node of each well. At the same node a temperature Dirichlet-type boundary condition is set to resemble the re-injection of cooled fluid. Fluid density contrasts and turbulent flow were not considered in our simulations, although the FRACTure code is able to do so. Viscosity and heat conduction of the fluid are temperature-dependent. For calibration the modeled pressures were fitted to measured hydraulic datasets. Here, focus was on the steady-state pressure, because for a long-term modeling it is sufficient to reproduce only the stationary pressure, rather than reproduce short-term transient pressure evolution. The replication of the initial pressure build-up in the beginning of circulation is considered only marginally. In doing so, permeability changes through thermal and poroelastic stresses are neglected. Furthermore chemical interaction such as precipitation, which might be relevant on the long-term, is neglected. As there was no hydraulic test of all four wells operating at the same time, we calibrate the pressures in GPK1-3 on the circulation test

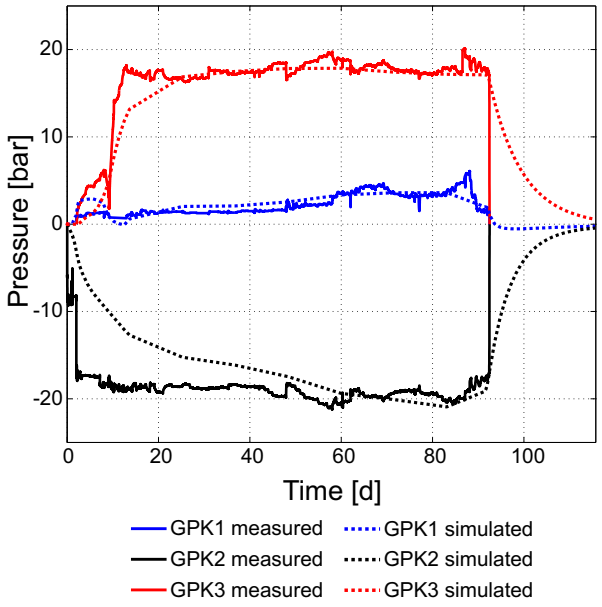

Figure 5: Results of the calibration using the circulation test between 05.01.2011 and 06.04.2001.

from early 2011 [Melchert, 2011] and pressure in GPK4 separately using the production test data from 2009 [Schindler, 2009]. The result of the calibration on the 2011 circulation test is shown in Figure 5.

The forward calibration on the transient pressures was done manually by changing the transmissivity of the fractures successively. The permeability of the host rock includes matrix and secondary fracture/fault systems. It was adapted first, because of its global impact on the reservoir. The calibrated host rock permeability is defined by the following permeability tensor:

assuming a viscosity of 2.31×10^{-4} Pa s, representing a fluid at 150 °C temperature, 35 MPa pressure and a salinity of 1.5 mol/kg [Kestin et al., 1981]. This is in reasonable good agreement with the permeability inversion by Shapiro et al. [1999] and Delépine et al. [2004], derived from recorded microseismicity of the GPK1 stimulation in 1993 for the upper reservoir and the GPK2 stimulation in 2000 for the deep reservoir, respectively. It also fits the measured permeability of the Soultz reservoir obtained from flow testing [Hettkamp et al., 1999]. The hydraulic properties of the fractures were defined in terms of isotropic transmissivity. The incorporated fracture network is dominating the fluid flow in the reservoir with a total transmissivity about one order higher than that of the matrix (Table 1). The major fracture GPK-FZ4770* connecting GPK2 and GPK3, is hydraulically divided into three parts, around GPK2, GPK3 and an outer zone to better represent the injectivities of these wells. When two fractures

Scenario	GPK1 [l/s]	GPK2 [l/s]	GPK3 [l/s]	GPK4 [l/s]
Standard 100%	+13	–26	+10	
Standard 75%	+9.75	–19.5	+7.5	
Standard 125%	+16.25	–32.5	+12.5	
Standard + GPK4	+17.8	–26	+14	–10
Without GPK1	–26	+13	+10	
Maximum	+24.58	–35	+17	–12

Table 2: Selected operation scenarios, production is negative, injection positive.

intersect one well, the relative transmissivity of these fractures is determined by the ratio of fluid influx as estimated from flow logs of these wells.

In order to assess the economic efficiency of the reservoir management, different operation scenarios were compared. Therefore a catalog of reasonable operation scenarios was defined. Operation is limited by a maximal injection pressure of 60 bar, as higher pressures cause excessive microseismicity [Cuenot et al., 2011]. Flow rate limits of 35 l/s are imposed by the well dimensions. GPK4 is restricted to a flow rate of only 12 l/s, as higher flow rates could not be achieved yet. As a reference scenario the current three wells operation (production of GPK2, injection in GPK1 and GPK3) is used (scenario Standard 100%). Additionally operation with three wells without using GPK1 is tested, because Genter et al. [2012] note the cooling of the producer GPK2 by the injector GPK1. Furthermore operation scenarios with all four wells were studied. A scenario with maximum flow rates defined according to the above limitations and operating all four well is tested. Table 2 summarizes the scenarios tested by our model. The difference between injected and produced thermal water, is provoked by a density contrast caused mainly by the withdrawal of heat for power generation. The presented ratio is determined after operation data from the power plant Each of these scenarios is run in the calibrated numerical model to generate input parameters for the economic calculations. The flow rates are prescribed as boundary conditions, as described above, the model determines the steady state pressure and the transient temperature fields.

5 Results and Discussion

In Figure 6 the results of the steady-state hydraulic modeling for the scenario "Maximum" are shown. The pressure drawdown around GPK2 and GPK4 and overpressure around GPK1 and GPK3 are visible. The pressure response in GPK3 and GPK4 is greater than in the other wells, although the flow rates are lower than in the other wells (Figure 6b). This results from higher transmissivity of the fractures linked to GPK1 and GPK2, representing the higher injectivity and productivity measured in those wells. This higher permeability is caused by the communication of GPK1 and GPK2 to the upper reservoir (GPK2 over casing restriction), which has a better permeability than the deeper reservoir [Hettkamp et al., 1999].

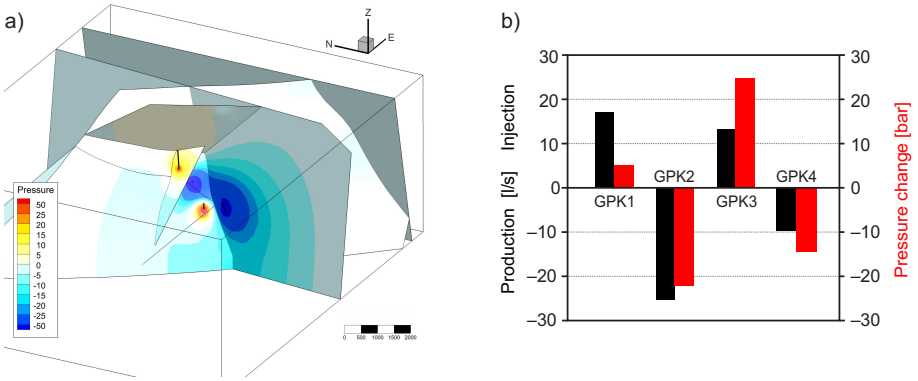

Figure 6: Pressure distribution in the reservoir at maximal flow rates after 30 years of constant production; black lines are wells GPK1-GPK4 from left to right; units are in meter, (b) pressure response in the wells due to fluid extraction and injection.

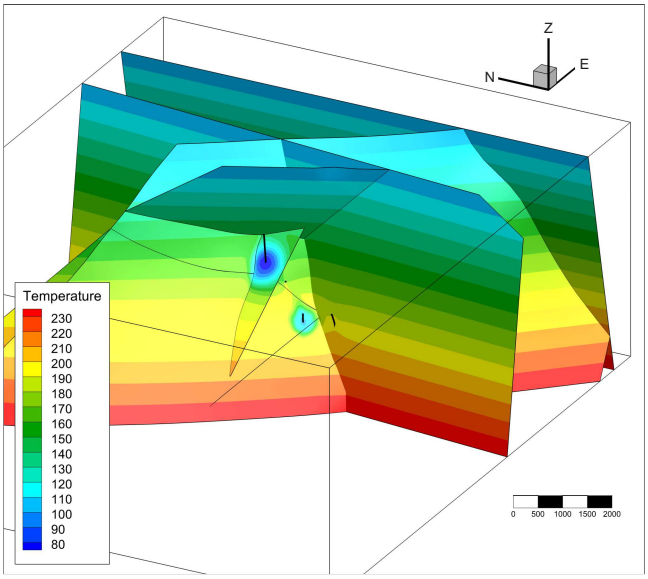

Figure 7: Temperature distribution in the reservoir at maximal flow rates after 30 years of constant production; black lines are wells GPK1-GPK4 from left to right; units are in °C.

Figure 7 shows the transient temperature distribution after 30 years of continuous operation with four wells after the scenario "Maximum". The temperature distribution shows a limited impact of the injection of cooled water. The impact is significantly greater along the fractures than the extent within the matrix. The diameter of the cooled area around GPK1 is about 1200 m, extending along the fracture MS-GPK3-2003a and much less towards the other wells. Because of the higher injection rate and the higher conductivity at GPK1 the cooled area is larger than that around GPK3.

The fractures, which are linked directly to the wells, dominate the behavior of the system. The most important structure is the fracture GPK3-FZ4770* connecting GPK2 and GPK3. It causes the direct connection between those two wells, mentioned by Sanjuan et al. [2006] and Sausse et al. [2010], and is also responsible for the good connection between GPK1 and GPK2 (via fracture MS-GPK3-2003a). This structure also has shown significant seismicity during stimulation periods [Cuenot et al., 2008, Schoenball et al., 2012] indicating major fluid flow. Analyzing tracer tests Sanjuan et al. [2006] proposed a large hydraulic loop connecting GPK4 and the other wells on an indirect fluid path. However, a good connection between GPK4 and the other wells is created by GPK3-FZ4770* as it is coupled with the fracture MS-GPK4-20045b (see Figure 4). For the low connectivity of GPK3 and GPK4 two possible arguments can be given: 1) the rather low fracture density and the absence of a large-scale fault intersecting GPK4 in the open-hole section [Dezayes et al., 2005, Sausse et al., 2010] and 2) the presence of a highly permeable anomaly, hydraulically disconnecting GPK3 and GPK4, as proposed by Kohl et al. [2006] from the observation of induced seismicity. Microseismicity was not present in this hypothetical structure, which could not be imaged by other techniques yet. The structure is striking N96°, dipping 64°.

The horst faults only have a limited hydraulic impact. They do not influence the temperature distribution but regulate the pressure distribution in the far-field. Although the fracture GPK1-FZ2120 is positioned in the cased section of GPK1, an impact on fluid injection in GPK1 is observed, as it is connected by the fracture MS-GPK3-2003a to the well. During drilling total mud loss was observed [Genter et al., 1997], indicating the high transmissivity of this fracture. The pressure in GPK1 is decreased by discharge of fluids into this fracture. The fracture PS3-int, almost perpendicular to the other structures and the main horizontal stress axis, has a negligible impact on the reservoir behavior.

Figure 8 shows the temperature evolution of the different operation scenarios of the fluid produced in GPK2 for up to 60 years. The current operation scenario "Standard 100%" is drawn in black. Common to all scenarios is a slight temperature increase of the produced fluids to about 180 °C. This is explained by fluid inflow from deeper sections of the reservoir and has also been observed. Depending on the scenario temperature starts to decline, resulting from the injection of the cooled fluids. However, after 60 years of constant production no sudden thermal breakthrough can be seen. The temperature decrease after 60 years of production is only about <2 K for the current operation scenario. The fluids produced at higher flow rates are colder, because of the higher amount

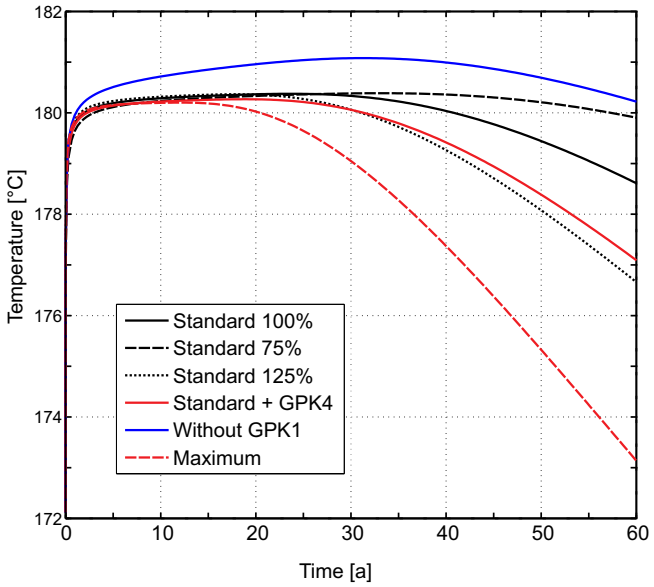

Figure 8: Temperature evolution of the produced fluid in GPK2.

of injected fluid. Operation without GPK1 results in a 1 K warmer thermal fluid and a retarded start of cooling. Genter et al., [2012] measure a cooling of the fluid produced from GPK2 by about 7 K when injecting in GPK1. From our modeling we can exclude this to be an effect of the reservoir. The cooling may be due to the interaction between the two wells at shallower depth, where the casings are separated by only few meters of rock or to production of still cooler fluids from earlier injections tests or stimulations. In case of simultaneous production from GPK2 and GPK4 (scenarios "Standard + GPK4" and "Maximum") the modeled production temperatures from GPK4 are slightly higher than from GPK2 because of colder fluid entering GPK2 through the leakage at 3880 m depth.

For model calibration and reservoir characterization only data from circulation tests between 2008 and 2011 could be used. However, the connection between GPK4 and the reservoir is still uncertain, because no hydraulic long-term circulation testing was done between GPK4 and the other wells. Therefore, the assessment of the well performance of GPK4 needs to be treated with care. A more refined calibration of the fracture network could be achieved using tracer test data [e.g. Gentier et al., 2010].

The buoyancy effect was neglected in the modeling approach. Assuming a mean transmissivity in the range between $6.8 \times 10^{-5}\,\mathrm{m^2\,s^{-1}}$ and $6.8 \times 10^{-4}\,\mathrm{m^2\,s^{-1}}$ (see Table 1) we can estimate a typical "forced fluid" head gradient in a distance of 100 m of 1×10^{-2} [-]. This is at least one order of magnitude larger than the "density driven" head gradient from buoyancy forces (assuming thermal expansion coefficient of $7 \times 10^{-4}\,\mathrm{K^{-1}}$ and a temperature dif-

ference of 50 K). Clearly the larger the distance from the injection well is, the lower the forced head gradient will be and the more dominant the buoyancy effect becomes. It is estimated that buoyancy will only establish at distances above 500 m distance from any well. This effect could potentially establish at large production periods under high flow rates and would cause a slightly lower thermal drawdown.

6 Economic consequences

Research at the geothermal power plant in Soultz focuses currently on sustainability and optimization. A profitable power production and an optimized reservoir management, depleting all existing wells, are key factors determining the (cost-) effectiveness and enhancement of the power plant. In the following section, the levelized cost of energy (LCOE) of different operation scenarios are compared to give a preliminary overview of the effectiveness of the different scenarios. The LCOE are calculated based on the annuity method as described in the German engineering code VDI 2067 [VDI, 2010]. Although calculations presented above were for 60 years of operation, we assume a depreciation of investments over an estimated lifetime of 30 years. During the reservoir operation further improvement of permeability of the reservoir through fracture creation or enhancement can be expected. This would result in pressure drawdown and higher fluid flow and cooler water will be produced. However, the effect of cost decrease through lower power consumption of the pumps prevails the effect of lower production temperature on income (see below); hence the LCOE will decrease with time. The temperature, flow and pressure drawdown and pressure raise obtained by the numerical model are used as input parameters. The goal is to improve the effectiveness of the project as it is. Disbursed investment costs such as exploration, drilling, stimulation and surface installations are not considered, while operation and maintenance (O&M) costs such as spare pumps and power self-consumption are taken into account. In this context, the production pump's energy demand and production pump investment are linked to the pressure drawdown in the reservoir and the power consumption of the injection pumps depends on pressure difference between reservoir and power plant. The power demand of the pumps was derived from reservoir parameters using the following equation:

$$P_{pump} = (TVP \cdot Q)/\eta,$$

with true vertical pressure TVP

$$TVP = p_{plant} + IDP \cdot g \cdot \rho + (IDP - WL) \cdot g \cdot \rho + \Delta p,$$

where IDP is installation depth of the pumps, WL is at-rest water level, Δp is pressure change due to injection or production and p_{plant} is operating pressure in the power plant. Injection pumps are only considered, if the pressure increase in the reservoir exceeds the operating pressure in the power plant. The calculated power of the pumps is presented in Table 4 Other O&M cost like personnel,

Fluid Density [kg/m3]	1064
Spec. heat capacity [J/(kg K)]	3950
Efficiency pumps [%]	72
Lifetime pumps [a]	1
Operation pressure, power plant [bar]	19
Gross efficiency power plant (thermal) [%]	10.5
Self-consumption power plant [% of thermal power]	5
return on capital [%]	9
Inflation [%]	2

Table 3: Input parameters for the economic calculations.

Scenarios	GPK1 [MW]	GPK2 [MW]	GPK3 [MW]	GPK4 [MW]
Standard 100%	0	0.223	0	
Standard 75%	0	0.151	0	
Standard 125%	0	0.306	0.007	
Standard + GPK4	0	0.223	0.013	0.074
Without GPK1	0.222	0.013	0	
Maximum	0	0.341	0.028	0.095

Table 4: Calculated values of the pumps; zero values = no pump needed, because power plant pressure exceeds injection pressure.

insurances, etc. are considered as well. All costs are inflation adjusted. The return on capital is 9%. Further input parameters are listed in Table 3.

In Figure 9 results of the economic comparison are shown. It is obvious, that an increase in production rate minimizes the LCOE. The LCOE decreases furthermore, if additional production rate is generated in GPK4. Interestingly, the scenario "Maximum" is not the optimal configuration, due to high pump costs and high self-consumption of the pumps. The scenario "Standard + GPK4" offers lowest LCOE from our catalog of scenarios; however a possible adjustment of flow rates might further decrease LCOE. The injection in GPK1 leads to a slight cooling of the fluid produced in GPK2, but neglecting of GPK1 as injector has negative effects on the LCOE (scenario "Without GPK1"). Therefore, instead of using GPK1 as an injector, GPK4 has to be used for injection. This requires an additional injection pump with higher cost and energy demand due to the low injectivity of GPK4 compared to GPK1. The additional costs raised through this pump prevail the additional produced energy, obtained due to slightly higher production temperature. Here, we have to keep in mind, that our model predicts only a cooling of about 1 K due to the injection in GPK1, instead of the reported 7 K (see above).

The decline of temperature and economic benefit over 30 years are only marginal. Therefore, the major factors influencing LCOE are investment cost and power consumption of the pumps, which have almost equal parts in the

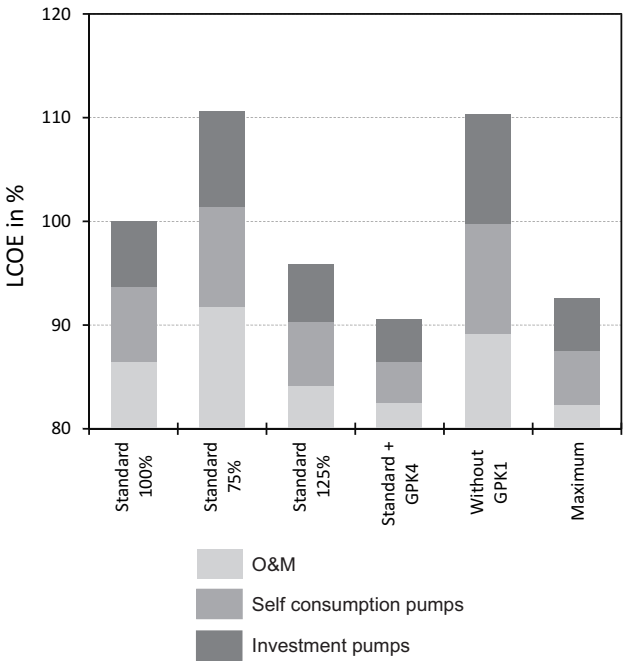

Figure 9: Results of the economic comparison of the different operation scenarios given in relationship to the current operation.

composition of costs (see Figure 9), whereas relative O&M costs decrease with increasing production rate. The composition of a whole exploitation costs of geothermal plant are documented in detail by Kölbel et al. [2011] and Guth [2011]. Optimization of pressure is much more important, even if temperature in the reservoir decreases slightly.

The study by Sanyal and Butler [2005] links reservoir management with economic considerations, focusing on the effects of stimulation and flow rates. Lacking direct operational experience and structural model, their study placed emphasis on theoretical considerations and optimizing reservoir design for an idealized reservoir. The use of a more generalized model generating the input parameter for the economic calculations has the advantage of comparability and transformation to other sides, so the developed guidelines have global validity. Our approach concentrates on the optimization of an existing site. It can either be used for optimization of an existing project, as in this case, or the development of a reservoir management strategy on basis of exploration data. Previous economic calculations at the Soultz site were conducted with the software code HDRec [Heidinger et al., 2006] by GTC Kappelmeyer GmbH. The code also links reservoir data with economic calculations to obtain the reservoir dependent economic output of the power plant. In contrast to the approach used here, characteristics of the reservoir are only considered in a simplified way.

Deterministic fractures, leakages and the complex 3D structure of the reservoir are not embedded in the model. Reservoir processes are calculated using analytical solutions leading to different results, especially for the temperature development, compared to the approach presented here. The economic description of the power plant is more extensive including more investment costs (e.g. wells, stimulation campaign costs, etc.), which are deliberately excluded in our approach.

According to Guth [2011] the three most influential cost factors of geothermal power production in low enthalpy regions are the lifetime of production pumps, the cost of drilling and the effectiveness of productivity and injectivity. The result of the calculations discussed above leads to a fourth major factor: multi-well systems have a significant impact on geothermal power production cost as well. While doublet systems tend to confine fluid circulation on single fracture planes connecting the wells, multi-well systems are characterized by fluid flow in the whole reservoir volume. Therefore multi-well systems have a much greater heat exchange surface. This leads to a better exploitation of the stored heat and longer lifetime of the geothermal reservoir. Furthermore, only multi-well systems allow for an actual optimization of the reservoir management, because of their greater flexibility to use wells either as producer or injector. Thus, the operation can be adapted to compensate for badly connected wells or exploit a well performance higher than expected during planning. For doublet systems, however there are little choices for reservoir operation with one injector and one producer. The system will always be limited by the least performing well.

7 Conclusion

We have demonstrated a workflow from a complex geological description of a geothermal reservoir to an economic performance quantification of the reservoir. Based on an existing geological model of the geothermal reservoir in Soultz-sous-Forêts, France, fractures dominating fluid flow were selected using flow and temperature logs. These fractures were implemented in a finite element numerical model. Steady-state pressure drawdown/raise through the reservoir operation, and transient production temperature changes were computed for different operation scenarios with constant prescribed flow rates. The output of the numerical model (flow rates, pressure and temperature changes) were transferred to an economic model based on the annuity method. Flow rate and temperature were used to calculate power production, while pressure determines invest and power consumption costs of the pumps. Additionally the model accounts for maintenance, operational and personnel costs. We compare different operation scenarios quantitatively in order to optimize the reservoir management at Soultz. We find a model with high, but not maximum production to have the lowest LCOE.

Our study shows the advantages of multi-well systems compared to doublet systems. Multi-well systems, such as Soultz, can be better optimized to obtain an increase of economic performance, due to the higher flexibility of operating

options are likely to activate multi fracture fluid loops and the corresponding spread of flow paths of the circulating fluid. A thermal breakthrough is likely to be postponed when accessing for multi fracture systems, which is, up to now, in good agreement with measurements in Soultz. Therefore long distances (1 km and more) separating the open-hole sections of the wells are not required. Shorter inter-well distances bear the possibility of a better enhancement of the reservoir by various stimulation techniques. By sensitivity runs effects of pressure variations on costs was clearly identified: these exceed the benefits of an increased temperature for power output. Again multi well systems could provide better performance than doublet systems used as one-fault systems.

Acknowledgements

The work was supported by EnBW Energie Baden-Württemberg AG. We thank GEIE Exploitation Minière de la Chaleur for providing data. Fruitful discussions with Adriana Guth and Eva Schill are greatly acknowledged. Especially we like to thank Tobias Hergert for his technical assistance. The authors thank the anonymous reviewers for valuable remarks, which helped to improve the manuscript.

References

Auradou, H. (2009), Influence of wall roughness on the geometrical, mechanical and transport properties of single fractures, *Journal of Physics D: Applied Physics*, 42(21), doi:10.1088/0022-3727/42/21/214015.

Bächler, D., T. Kohl, L. Rybach (2003), Impact of graben-parallel faults on hydrothermal convection - Rhine Graben case study, *Physics and Chemistry of the Earth*, 28, 431 - 441, doi:10.1016/S1474-7065(03)00063-9.

Baillieux, P., E. Schill, C. Dezayes (2011), 3D structural regional model of the EGS Soultz site (northern Upper Rhine Graben): insights and perspectives, In: *36th Workshop on Geothermal Reservoir Engineering*, Stanford University, CA, USA.

Barton, C. A., M.D. Zoback, D. Moos (1995), Fluid flow along potentially active faults in crystalline rock, *Geology*, 23(8), 683 - 686, doi:10.1130/0091-7613(1995)023¡0683:FFAPAF¿2.3.CO;2.

Baujard, C. and D. Bruel (2006), Numerical study of the impact of fluid density on the pressure distribution and stimulated volume in the Soultz HDR reservoir, *Geothermics*, 35, 607 - 621, doi:10.1016/j.geothermics.2006.10.004.

Blumental, M., M. Kuhn, H. Pape, V. Rath, C. Clauser, (2007), Hydraulic model of the deep reservoir quantifying the multi-well tracer test, In: *EHDRA scientific conference 28 - 29 June 2007*, Soultz-sous-Forêts, France.

Cantini, S., (2006), GEIE Well GPK-4 Flow Log - leak detection, Technical report Schlumberger for GEIE EMC.

Cornet, F.H., T. Bérard, S. Bourouis, (2007), How close to failure is a granite rock mass at a 5km depth?, *International Journal of Rock Mechanics and Mining Sciences*, 44, 47 - 66,doi:10.1016/j.ijrmms.2006.04.008.

Cuenot, N., J. Charléty, L. Dorbath, H. Haessler (2006), Faulting mechanisms and stress regime at the European HDR site of Soultz-sous-Forêts, France, *Geothermics*, 35, 561 - 575, doi:10.1016/j.geothermics.2006.11.007.

Cuenot, N., M. Del Mar Mesa Salgado, C Naville, A. Gérard, J. Place (2007), Soultz VSP 2007 campaign in GPK3 and GPK4: operation report and preliminary results, In: *EHDRA scientific conference 28 - 29 June 2007*, Soultz-sous-Forêts, France.

Cuenot, N., C. Dorbath, L. Dorbath (2008), Analysis of the Microseismicity Induced by Fluid Injections at the EGS Site of Soultz-sous-Foreˆts (Alsace, France): Implications for the Characterization of the Geothermal Reservoir Properties, *Pure Appl. Geophys.* 165, 797 - 828, doi:10.1007/s00024-008-0335-7.

Cuenot, N., M. Frogneux, C Dorbath, M Calo (2011), Induced microseismic activity during recent circulation tests at the EGS site of Soultz-sous-Forêts (France), *36th Workshop on Geothermal Reservoir Engineering*, Stanford University, CA, USA.

Delépine, N., N. Cuenot, E. Rothert, M. Parotidis, S. Rentsch, S.A. Shapiro (2004), Characterization of fluid transport properties of the Hot Dry Rock reservoir Soultz-2000 using induced microseismicity, *Journal of Geophysics and Engineering*, 1, 77 - 83, doi:10.1088/1742-2132/1/1/010.

Dezayes, C., T. Villemin, A. Genter, H. Traineau, J. Angelier (1995), Analysis of fractures in boreholes of the Hot Dry Rock project at Soultz-sous-Forêts (Rhine Graben, France). *Sci. Drilling*, 5, 31 - 41.

Dezayes, C., A. Genter, S. Gentier (2004), Fracture network of the EGS Geothermal Reservoir at Soultz-sous-Forêts (Rhine Graben, France), In: *Geothermal Resources Council*, 213-218, Palm Springs, CA, USA.

Dezayes, Ch., Ph. Chèvremont, B. Tourlière, G. Homeier, A. Genter (2005), Geological study of the GPK4 HFR borehole and correlation with the GPK3 borehole (Soultz-sous-Forêts, France). Open file report BRGM/RP-53697-FR, p. 94, BRGM, Orléans, France.

Dezayes, C., A. Genter, B. Valley (2010), Structure of the low permeable naturally fractured geothermal reservoir at Soultz, *C. R. Geoscience*, 342, 517 - 530, doi:10.1016/j.crte.2009.10.002.

Dorbath, L., N. Cuenot, A. Genter, M. Frogneux (2009), Seismic response of the fractured and faulted granite of Soultz-sous-Forêts (France) to 5 km deep

massive water injections, *Geophys. J. Int.*, 177, 1 - 23, doi:10.1111/j.1365-246X.2009.04030.x.

Evans, K.F., H. Moriya, H. Niitsuma, R.H., Jones, W.S. Phillips, A., Genter, J. Sausse, R. Jung, R. Baria (2005), Microseismicity and permeability enhancement of hydrogeologic structures during massive fluid injections into granite at 3 km depth at the Soultz HDR site, *Geophys. J. Int.*, 160, 388 - 412, doi:10.1111/j.1365-246X.2004.02474.x.

Geiermann, J. and E. Schill (2010), 2-D Magnetotellurics at the geothermal site at Soultz-sous-Forêts: Resistivity distribution to about 3000 m depth, *C. R. Geoscience*, 342, 587 - 599, doi:10.1016/j.crte.2010.04.001

Genter, A., H. Traineau, C. Dezayes, P. Elsass, B. Ledésert, A. Meunier, T. Villemin (1995), Fracture analysis and reservoir characterization of the granitic basement in the HDR Soultz project (France), *Geotherm. Sci. Technol.*, 4(3), 189 - 214.

Genter, A., H. Traineau, D. Artignan (1997), Synthesis of geological and geophysical data at Soultz-sous-Forêts (France), Open file report BRGM/RR-39440-FR, p. 36, BRGM, Orléans, France.

Genter, A., G. Homeier, P. Chévremont, H. Tenzer (1999), Deepening of GPK-2 HDR borehole, 3880-5090 m (Soultz-sous-Forêts, France). Geological monitoring, Open file report BRGM/RR-40685-FR, p. 81, BRGM, Orléans, France.

Genter, A., K. Evans, N. Cuenot, D. Fritsch, B. Sanjuan (2010), Contribution of the exploration of deep crystalline fractured reservoir of Soultz to the knowledge of enhanced geothermal systems (EGS), *C. R. Geoscience* 342, 502 - 516, doi:10.1016/j.crte.2010.01.006

Genter, A., N. Cuenot, X. Goerke, B. Melchert, B. Sanjuan, J. Scheiber (2012), Status of the Soultz Geothermal Project During Exploitation between 2010 and 2012, In: *37th Workshop on Geothermal Reservoir Engineering*, Stanford University, CA, USA.

Gentier, S., X. Rachez, T.D. Tran Ngoc, M. Peter-Borie, C. Souque (2010), 3D flow modelling of the medium-term circulation test performed in the deep geothermal site of Soultz-sous-Forêts (France), In: *World Geothermal Congress 25 -30 April 2010*, Bali, Indonesia.

Gérard, A., J. Baumgärtner, R. Baria, R. Jung (1997), An attempt towards a conceptual model derived from 1993-1996 hydraulic operations at Soultz, In: *International Geothermal Symposium 11-12 March 1997*, Sendai, Japan.

Guth, A. (2011), Monte-Carlo-Simulation der Stromgestehungskosten für Geothermie im Oberrheingraben, B.Sc. thesis, Institute of Industrial Productions (IIP), KIT, Karlsruhe, Germany.

Haas, J.-O. and C.R. Hoffmann (1929), Temperature gradient in Pechelbronn oil bearing region, lower Alsace: its determination and relation to oil reserves. *Bull. Amer. Assoc. Petr. Geol.*, 13(10), 1257 - 1273.

Heidinger, P., J. Dornstädter, A. Fabritius (2006), HDR economic modelling: HDRec software, *Geothermics*, 35, 683 - 710, doi:10.1016/j.geothermics.2006.10.005.

Hettkamp, T., G. Fuhrmann, F. Rummel (1999), Hydraulic properties in the Rhine Graben basement material, *Bulletin d'Hydrogéologie Centre d'Hydrogiologie*, Université de Neuchatel, 17, 143-150.

Hooijkaas, G.R., A. Genter, C. Dezayes (2006), Deep-seated geology of the granite intrusions at the Soultz EGS site based on data from 5 km deep boreholes, *Geothermics*, 35(5-6), 484 - 506.

IEA International Energy Agency (2011), Technology Roadmap: Geothermal Heat and Power, Paris, France.

Jung, R., M. Schindler, P. Nami, T. Tischner (2010), Determination of flow exits in the Soultz borehole GPK2 by using the brine displacement method, *C. R. Geoscience*, 342, 636 - 643, doi:10.1016/j.crte.2009.06.002

Kestin, J., H.E. Khalifa, R.J. Correia (1981), Tables of the dynamic and kinematic viscosity of aqueous NaCl solutions in the temperature range 20 - 150 °C and the pressure range 0.1 - 35MPa, *Journal of physical and chemical reference data*, 10(1).

Kölbel, T., L. Eggeling, W. Münch, P. Schlagermann (2011), Geothermal achieving competitivity: Cost of power generation, paper presented at *Geopower Europe 6 - 7 December 2011*, Milan, Italy.

Kohl, T. and R.J. Hopkirk (1995), "FRACTure" a simulation code for forced fluid flow and transport in fractured porous rock, *Geothermics* 24, 345 - 359, doi:10.1016/0140-6701(95)96651-R.

Kohl, T., C. Baujard, T. Mégel (2006), Conditions for mechanical re-stimulation of GPK4, In: *EHDRA scientific conference 15 - 16 June 2006*, Soultz-sous-Forêts, France.

Kohl, T. and T. Mégel (2007), Predictive modeling of reservoir response to hydraulic stimulations at the European EGS site Soultz-sous-Forêts, *International Journal of rock mechanics and mining science*, 44, 1118 - 1131, doi:10.1016/j.ijrmms.2007.07.022

Kosack, C., C. Vogt, V. Rath, G. Marquart (2010), Stochastic estimates of the permeability field of the Soultz-sous-Forêts geothermal reservoir - comparison of bayesian inversion, MC geostatistics, and EnKF assimilation, In: *European Geosciences Union General Assembly*, 2-7 May 2010, Vienna, Austria.

Kruck, C., T. Kölbel, L. Eggeling, T. Weimann (2011), Strom aus Geothermie: Kosten und Kostensenkungspotenziale, *bbr Fachmagazin für Brunnen - und Leitungsbau*, Sonderheft Geothermie 62, 56 - 62.

Le Carlier, Ch., J.-J. Royer, E.L. Flores (1994), Convective heat transfer at the Soultz-sous-Forêts Geothermal Site: implications for oil potential, *First break*, 12(11), 553 - 560, doi10.3997/1365-2397.1994033.

Melchert, B. (2011), Monthly hydraulic report (Feb. - Mar. 2011) at the EGS Soultz site, 3, BGR, Hannover, Germany.

Pfender, M., P. Nami, T. Tischner, R. Jung (2006), Status of the Soultz deep wells based on low rate hydraulic tests and temperature logs, In: *EHDRA Scientific Conference 15 - 16 June 2006*, Soultz-sous-Forêts, France.

Place, J., M. Diraison, C. Naville, Y. Géraud, M. Schaming, C. Dezayes (2010), Decoupling of deformation in the Upper Rhine Graben sediments. Seismic reflection and diffraction on 3-component Vertical Seismic Profiling (Soultz-sous-Forêts area), *C. R. Geoscience*, 342, 575 - 586, doi:10.1016/j.crte.2010.01.001.

Place, J., J. Sausse, J-M. Marthelot, M. Diraison, Y. Géraud, C. Naville (2011), 3-D mapping of permeable structures affecting a deep granite basement using isotropic 3C VSP data, *Geophys. J. Int.*, 186, 245 - 263, doi:10.1111/j.1365-246X.2011.05012.x

Sanyal, S.K. and S.J. Butler (2005), An Analysis of Power Generation Prospects From Enhanced Geothermal Systems, In: *World Geothermal Congress 24 - 29 April 2005*, Antalya, Turkey.

Sanjuan, B., J.-L. Pinault, P. Rose, A. Gérard, M. Brach, G. Braibant, C. Crouzet, J.-C. Foucher, A. Gautier, S. Touzelet (2006), Tracer testing of the geothermal heat exchanger at Soultz-sous-Forêts (France) between 2000 and 2005, *Geothermics*, 35, 622 - 653, doi:10.1016/j.geothermics.2006.09.007

Sardini, P., B. Ledésert, G. Touchard (1997), Quantification of microscopic porous networks by image analysis and measurements of permeability in the Soultz-sous-Forêts granite (Alsace, France), in *Fluid flow and Transport in rocks*, 171 - 189, B. Jamtvei, B. W. D. Yardley. London, Great Britain

Sausse, J. and A. Genter (2005), Types of fracture permeability in granite, in Special Publication of the Geological Society of London, 240, 1 - 14, P.K. Harvey, T.S. Brewer, P.A. Pézard, V.A. Petrov (Eds.), London, Great Britain, doi:10.1144/GSL.SP.2005.240.01.01.

Sausse, J., M. Fourar, A. Genter (2006), Permeability and alteration within the Soultz granite inferred from geophysical and flow log analysis, *Geothermics*, 35, 544 - 560, doi:10.1016/j.geothermics.2006.07.003.

Sausse, J., C. Dezayes, L. Dorbath, A. Genter, J. Place, (2010), 3D fracture zone network at Soultz based on geological data, Image logs, mi-

croseismic events and VSP results, C. R. Geoscience, 342, 531 - 545, doi:10.1016/j.crte.2010.01.011.

Schindler, M., P. Nami, R. Schellschmidt, D. Teza, T. Tischner (2008), Summary of hydraulic stimulation operations in the 5 km deep crystalline HDR/EGS reservoir at Soultz-sous-Forêts, In: *33th Workshop on Geothermal Reservoir Engineering*, 28 - 30 Jan. 2008, Stanford University, CA, USA.

Schindler, M. (2009), Hydraulic data recorded during the three circulations with down-hole pumps at Soultz, Rapport public GEIE np RAP 71 000 V00, p. 20, GEIE, Soultz-sous-Forêts, France

Schoenball, M., C. Baujard, T. Kohl, L. Dorbath (2012), The role of triggering by static stress transfer during geothermal reservoir stimulation, *J. Geophys. Res.*, 117(B9), B09307. doi:10.1029/2012jb009304.

Shapiro, S. A., P. Audigane, J.-J. Royer (1999), Large-scale in situ permeability tensor of rocks from induced microseismicity, *Geophys. J. Int.*, 137(2), 207 - 213.

Sulzbacher, H. and R. Jung (2005), Thermo-hydraulic modelling results of the deep reservoir in the Soultz and consequences for the design of commercial HDR-Systems, In; *EHDRA scientific conference 17 - 18 March 2005*, Soultz-sous-Forêts, France

Tester, J.W., B.J. Anderson, A.S. Batchelor, D.D. Blackwell, R. DiPippo, E.M. Drake, J.D. Garnish, B. Livesay, M.C. Moore, K. Nochols, S. Petty, M.N. Toksoez, R.W.J. Veatch (2006), The Future of Geothermal Energy: Impact of Enhanced Geothermal Systems (EGS) on the United States in the 21st Century, 372 p., Massachusetts Institute of Technology, Idaho Falls, ID, USA.

VDI (2010), VDI 2067: Wirtschaftlichkeit gebäudetechnischer Anlagen - Grundlagen und Kostenberechnung, Verein Deutscher Ingenieure (VDI), VDI Verlag GmbH, Düsseldorf, Germany September 2010.

Vogt, C., C. Kosack, G. Marquart (2012a), Stochastic inversion of the tracer experiment of the enhanced geothermal system demonstration reservoir in Soultz-sous-Forêts - Revealing pathways and estimating permeability distribution, *Geothermics*, 42, 1 - 12, doi:10.1016/j.geothermics.2011.11.001.

Vogt, C., G. Marquart, C. Kosack, A. Wolf, C. Clauser (2012b), Estimating the permeability distribution and its uncertainty at the EGS demonstration reservoir Soultz-sous-Forêts using the ensemble Kalman filter, *Water Resources Research*, 47, W08517, doi:10.1029/2011WR011673

Ziegler, P. (1994), Cenozoic rift system of western and central Europe: an overview. *Geologie en Mijnbouw* 73, 99 - 127.